Applied Physics A (2022) 128:404
https://doi.org/10.1007/s00339-022-05540-x

Applied Physics A
Materials Science & Processing

A label-free Acetone based SnO_2 nanowire network sensor at room temperature

Estácio P. de Araújo[1] · Cleber A. Amorim[2] · Adryelle N. Arantes[1,3] · Adenilson J. Chiquito[1]

Received: 19 January 2022 / Accepted: 28 March 2022 / Published online: 16 April 2022
© The Author(s), under exclusive licence to Springer-Verlag GmbH, DE part of Springer Nature 2022

Abstract
Acetone is a toxic gas employed in several pharmaceutical and commercial preparations, circumstances that demand efficient exposure control methods. Quasi-one-dimensional SnO_2 (n-type) is a remarkable material for such purpose. In this work, we discuss the characteristics of an Acetone gas sensor built in a metal–semiconductor-metal (MSM) architecture, using a SnO_2 nanowire network as an activity layer. The crystallographic information was confirmed using XRD and found out to be monocrystalline and in a rutile structure. SEM images confirmed that the desired nanowire morphology was obtained. The Acetone gas concentration was varied from 50 to 970 PPM and sensor response ranged between 9 and 32% at room temperature. By operating in 0.1 V, with a sensitivity of 49% in 970 PPM, an optimized regime of the gas sensor was achieved. The rise time varied between 8.7 s and 13 s and decay time ranged between 48.1 s and 142.7 s. In addition, we demonstrated fast response time, stability and reproducibility, all essential features for a high-quality sensor.

Keywords SnO_2 nanowire network · Acetone gas sensor · Room temperature

1 Introduction

Acetone is a volatile organic compound (VOC) mostly used in industrial processes as a solvent in pharmaceutical and commercial preparations. Similarly to other VOCs, issues may arise regarding direct human contact. Beyond Acetone's toxicity, that may cause eye irritation, headaches and nausea, one must acknowledge its high cancer-causing potential [1], which emphasizes the need of exposure control methods. In addition, studies have suggested that breath gases, such as Acetone, can be related to blood glucose and blood ketone levels in adults with types 2 and 1 diabetes [2], results that also motivate the development of an Acetone sensor, to be employed as a non-invasive technique of diabetes monitoring.

As means to respond to this demand, one must consider assembling an Acetone sensor that features high selectivity, sensitivity, simplicity in fabrication and low power consumption. For such purpose, Transparent Conducting Oxides (TCO) have been widely employed [3]. From this class of materials, one can highlight CuO, ZnO, ITO, TiO_2 and SnO_2 [4–8], which have already been tested for Acetone sensing, among other purposes, e.g., flame detection, light, pH and biosensors [9–11]. Tin dioxide (SnO_2) is an n-type semiconductor that presents a wide bandgap around 3.6 eV, at room temperature. Furthermore, SnO_2 presents unique properties that provide the basis for electron transport in hole blocking layers printed, in particularly one-dimensional morphology, applications nanowires manufactured via printing and laser irradiation [12]. In addition, they can perform electron injection and charge recombination functions for a range of device architectures [13]. Concerning gas sensing, nano-structured SnO_2 has already been proven suitable for a wide range of different gases [14].

Generally, a gas sensor performance and limits for detection are measured by its selectivity, rise and decay time, reproducibility, stability, power consumption and operation temperature. Operation temperature of gas sensors can vary

✉ Estácio P. de Araújo
estacio.paiva@gmail.com

[1] NanOLaB, Physics Department, Federal University of São Carlos, Rodovia Washington Luiz, Km 235, Monjolinho, São Carlos, São Paulo 13565-905, Brazil

[2] School of Sciences and Engineering, Av. Domingos da Costa Lopes, São Paulo State University (Unesp), 780 Jardim Itaipu, Tupã, SP CEP 17602-496, Brazil

[3] Section of Nuclear Medicine, Department of Internal Medicine, Ribeirão Preto Medical School, University of São Paulo, Ribeirão Preto, São Paulo, Brazil

according to the environment temperature. At higher temperatures, they can achieve great results and fast response time. On the other hand, a high temperature may cause structural transformations, such as phase separation, electrical contact degradation and decrease of device's lifetime [15–17]. Given that, even with a lower response time, a room temperature device is preferable. Regarding those parameters, studies demonstrated that one-dimensional morphology, such as SnO_2 nanowires (NW), enhances the sensor response even at room temperature since the surface-to-volume ratio increases and the surface interactions begin to rule the device's behavior [18]. In such case, the oxygen adsorbent sites and defects in the surface can control the conductance of the active channel of detection.

For a SnO_2 NW network, during the synthesis process, different sizes and lengths of nanowires are grown and countless junctions between them are formed. As a consequence of these junctions, potential barriers arise on the interfaces and rule the charge transport. Thus, one could say that a percolative pathway describes the electrons' movement throughout the network [19]. When considering a single NW, obviously, there are no junctions formed and electrons can travel in the conductive channel without obstacles. Withal, in both cases, there is no regular surface arrangement due to crystal lattice symmetry breaking, leading to defects and vacancy sites that enable their employment, as a network or single NW, for gas sensing.

Among Acetone gas sensors' physicochemical properties, the main mechanism that controls detection is related to the effect of oxygen molecules adsorption/desorption on surface, variations that can modify barrier height and depletion layer width. Therefore, under a given value of gas concentration, SnO_2 NWs' surface responds with a corresponding surface charge density change that modifies the local electric field and, consequently, the electrical current.

Studies with different TCOs employed as gas sensors can be found in the literature. For instance, Saraswati and Ruma have achieved a response that ranged between 0.6 and 7% for 500–7000 PPM concentration of Acetone, for a device with a CuO NW network, with Rise and Decay times of 250 s and 300 s (for 1000 PPM), respectively [4]. Regarding response time, Karthika et al. have reported an Acetone gas sensor using a ZnO thin film with Rise and decay time of 34 s and 40 s ($\tau_R = 34$ and $\tau_D = 40$ s) [20]. Jie Zhao et al. built a SnO_2 thin film by a Sol–gel method that presented a sensitivity of about 12 (ratio between gas on and off conditions) under a 1000 PPM Acetone concentration. Rise and decay times were smaller than 20 s and 60 s, respectively [21]. Zijing Wang et al. reported an Acetone gas sensor composed by a p–n junction nanocomposites of SnO-SnO_2/$Ti_3C_2T_x$, operating at room temperature. Sensor response presented a sensitivity gain about 12.1 and rise and decay times were 18 s and 9 s, respectively [22]. According to our knowledge, SnO_2 NW devices as an Acetone gas sensor, at room temperature, have not been explored up to now.

In this work, we discuss the gas sensing properties of a SnO_2 nanowire network employed as an Acetone gas detector. The electrical characterization techniques chosen for such studies were the current–voltage (I–V) and current–time (I-t) curves with and without the presence of Acetone gas. Acetone gas detection ranged from 50 to 970 PPM, with a sensor response of 9% and 31%, respectively. As means to enhance the sensibility, different values of applied voltage were tested, from 0.1 V to 9 V. An improvement was noticed with lower applied voltages for a 970 PPM concentration, with a rise time between 9 and 13 s and decay time between 50 and 150 s. By comparison, our devices reached an excellent result, with high sensibility, simplicity in the fabrication process, free of cleanroom environment facilities and photolithography techniques.

2 Materials and methods

Tin Dioxide NWs were synthesized by the vapor–liquid-solid (VLS) growth technique. This mechanism is aided by metal catalyst nanoclusters, which are employed to serve as preferential sites for adsorption of vapor phase components, driving a one-dimensional growth structure. At first, thin films of gold (15 Å) were deposited (Edwards 306 coating system) in Si/SiO_2 substrates (oxide layer 500 nm thick) to generate the nanoclusters. The synthesis was performed in a tube reactor (Lindberg blue M), where a high purity Tin powder (0.1 g, Aldrich, purity > 99.99%) was located in center of reactor, in an alumina crucible, heated up to 950° C (heating rate of 19 °C/min) and kept at this value for 50 min. An Argon/Oxygen mixture with a constant flow of 15/8 sccm (Mass Flow MKS 1149) was maintained along of synthesis, to ensure the vapor transport to the synthesis region, with controlled pressure by a vacuum pump around 350 mbar. Afterwards, by Scanning Electron Microscopy (SEM, JEOL JSM 6510, operated at 20 kV) and X-Ray Diffraction (XRD, Rigaku D/max-2500, Cu-Kα radiation) the structural properties of the as-grown samples were analyzed.

Acetone gas sensor was built based on a metal–semiconductor-metal (MSM) architecture, which consists of a semiconductor material in contact with two metallic electrodes [23]. The semiconductor is the SnO_2 NW network, whereas the metallic electrode was chosen to be made of Indium (≈ 3 mm^2), highlighted in Fig. 1 (green arrow). Furthermore, it is a simple process, cheap and with no need for a complex photolithography process, neither clean room environment.

Figure 1 depicts a setup configuration assembled for the Acetone vapor to reach the chamber. Nitrogen cylinder (impurity < 1 PPM of O_2) was connected in two different lines. One line was employed to assist the Acetone vapor

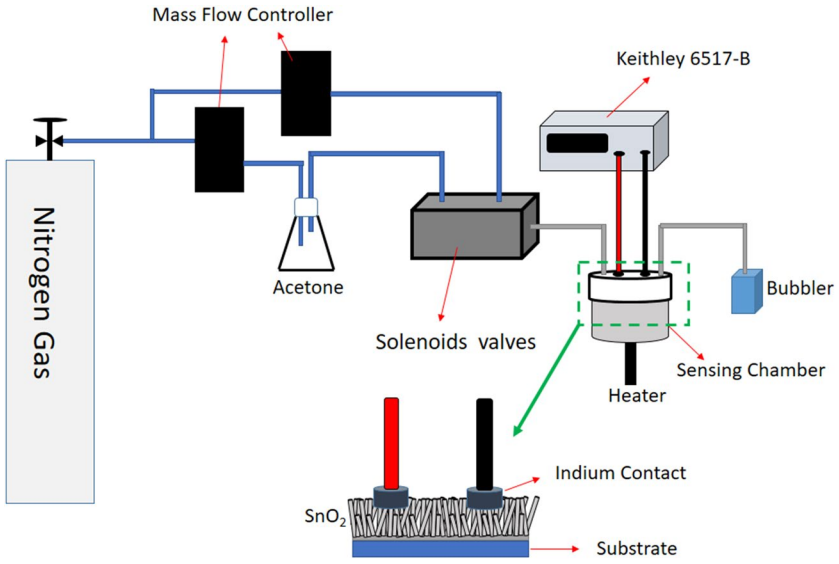

Fig. 1 Schematic representing the setup configuration used for Acetone detection

transport, whereas the second was used for pure Nitrogen. The flow was controlled (mass flow MKS 1149) to enable to estimate the Acetone concentration by Eq. 1 [24]:

$$[\text{conc}]_f = \frac{V_{\text{gas}}}{V_{\text{gas}} + V_{N_2}}[\text{conc}]_{\text{gas}}, \tag{1}$$

with

$$[\text{conc}]_{\text{gas}} = \frac{m}{V_c}\frac{1}{MW}V_i.10^6, \tag{2}$$

where V_{gas} is the Acetone gas' volumetric flow rate (sccm), V_{N_2} is the Nitrogen gas' volumetric flow rate (sccm), m is the evaporated acetone's mass in 60 s, V_c is the chamber's volume (0.25 l), MW represents the Acetone's molecular mass (58.08 g/mol) and V_i is the ideal gas volume (22.4 l). Solenoids valves are used to start and stop the flow, in a controlled manner, at the sensing chamber. The sensing chamber, where the samples are placed in, is connected to a Keithley 6517-B, which is employed as both voltage source and current detector. The gas that flows out of the sensing chamber finally reaches the bubbler, that acts as a filter.

3 Results and discussion

Figure 2a presents a typical XDR pattern recorded from the as-grown samples. The Miller indices were indicated in each diffraction peak. All diffraction peaks indexed show rutile-like peaks (JCPDS 41–1445) [25] as expected for the tetragonal structure of SnO_2 ($a = 4.738$ Å and $c = 3.187$ Å) within the $P4_2/mm$ spatial group. No obvious reflection peaks from impurities, such as unreacted Sn or other tin oxides, were detected, indicating the high purity of the as-grown samples.

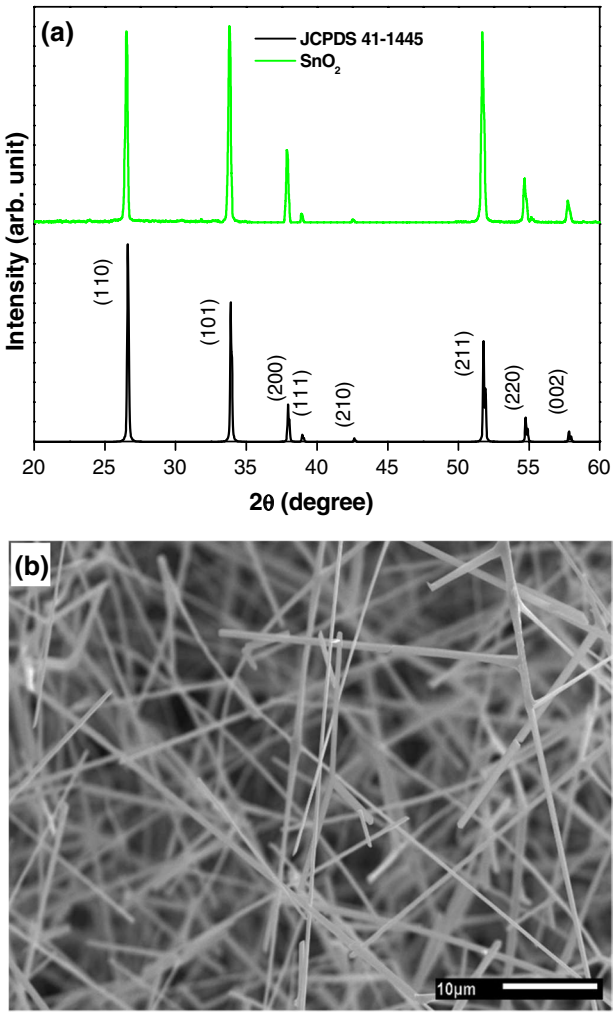

Fig. 2 **a** XDR pattern of as grow samples (black) displaying rutile like peaks (JCPDS 41–1445, green), **b** SEM image of the nanowire network

A scanning electron microscopy (SEM) image of VLS synthesis is present in Fig. 2b. The SEM image reveals the randomized nanostructures' growth direction. Statistical analysis of many SEM images shows that the average diameter of these nanowires varies from 50 to 800 nm and lengths ranging from 10 to 800 µm. Cross-sections mostly displaying rectangular geometry were observed. Moreover, it is also possible to observe multiple branched nanowires that can arise during the synthesis process of one-dimensional nanostructures, known as self-catalytic dendrites [26], although there is no interference in our results.

I–V curve of SnO_2 NW's network device is displayed in Fig. 3, at environment condition and after heating under a N_2 flow. At environment condition, the surface is filled with adsorbed oxygen, causing electrons to be trapped in adsorbent sites, resulting in a low electrical current. When under N_2 flow, the process involves heating the samples until it reaches 100 °C, for about 10 min, and then wait for their return to room temperature. This process aims to modify the surface states and consequently, decrease the space charge region, which in turn leads to increased electrical current. Furthermore, Fig. 3 also depicts an Ohmic-like behavior at the metal–semiconductor interface (MS), however, linearity does not imply barrier absence [23].

Figure 4 depicts the sensor response as a function of time under different Acetone concentrations, operating at an applied voltage of 1 V. The gas response values of the samples used in this work were given by the formula: $(I_g–I_{N2})/I_{N2}$, where I_{N2} represented the current value of the sensing material in nitrogen, I_g represented the current value of the sensing material in Acetone gas. The sensor response achieved 9% and 32% for 50 and 970 PPM, respectively. The increased sensor response as a function Acetone

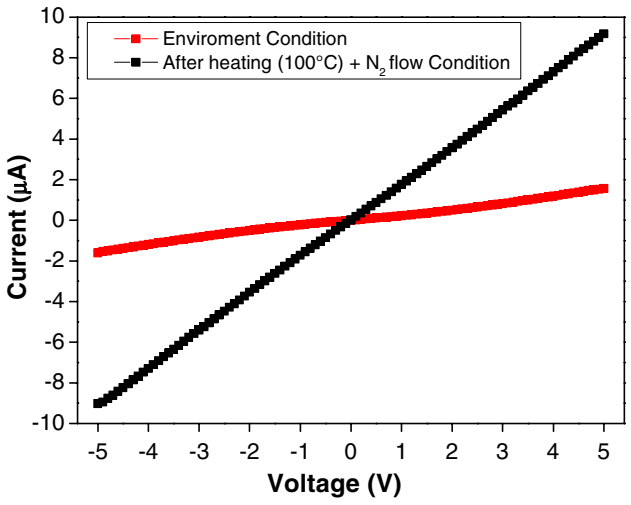

Fig. 3 I–V curve for the SnO_2 nanowire network gas sensor in: environment condition (red) and after heating (100 °C) under N_2 flow condition (black)

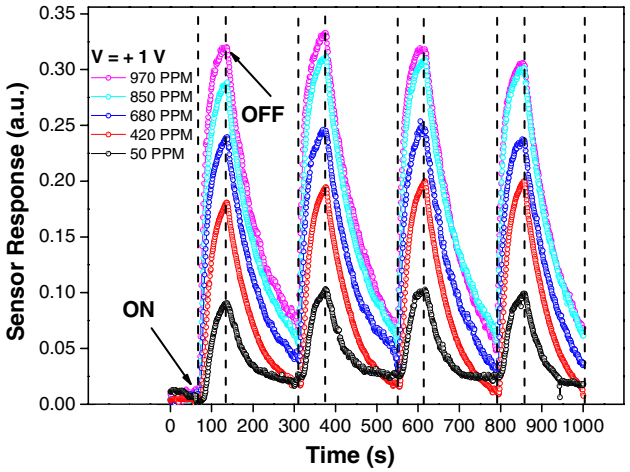

Fig. 4 Sensor response-time comparing different concetration of Acetone gas: 970 PPM (pink), 850 PPM (cyan), 680 PPM (blue), 420 PPM (red) and 50 PPM (black). All under the same applied voltage value of + 1 V.Fig. 5. **a** I-t characteristics of the device when different voltage: 9 V (red), 6 V (dark yellow), 3 V (blue), 1 V (green), 0.5 V (red) and 0.1 V (black). **b** Sensor Response-time under different voltage values: 0.1 V (black), 0.5 V (red), 1 V (green), 3 V (blue), 6 V (dark yellow) and 9 V (pink). All under the same Acetone concentration of 970 PPM

concentration is expected since it is related to the Acetone amount that is able to remove Oxygen from the surface. At the first 60 s, the device is only under N_2 flow. Afterwards, at 60 s, the sensor is exposed to the Acetone vapor during 60 s. At 180 s, the Acetone vapor is turned off and only N_2 flow is present in the chamber. This cycle totals 240 s.

Since stable and reproducible results were obtained for the acetone gas sensor, other voltage values were investigated as means to achieve the best performance and get an optimized regime. Figure 5a depicts the logarithmic current as a function of time, with different applied voltage as follows: 9 V, 6 V, 3 V, 1 V, 0.5 V and 0.1 V for an Acetone concentration of 970 PPM. For all applied voltage, an increase of the electrical current while there was an Acetone flow inside the chamber was noticed, highlighting that regardless of the applied voltage used, the shape of the response did not change, displaying stability. Detailed sensor response data are presented in Fig. 5b. Comparing the curves, one can note that the lowest values of applied voltage resulted in the highest sensibility. It was observed that a lower quantity of available electrons flowing through the SnO_2 NW network can improve the gas sensing since it starts with a sensor response around 0.32 at 9 V and increases up to 0.49 at 0.1 V. The additional non-linear effects due to the high electric field can decrease the gas detection effect. Thus, the detection can be more clearly perceived at low voltages.

Analyzing separately all curves in Fig. 5b, it was possible to find a rise time (τ_R) and decay time (τ_D) by using Eq. (3) and (4), respectively:

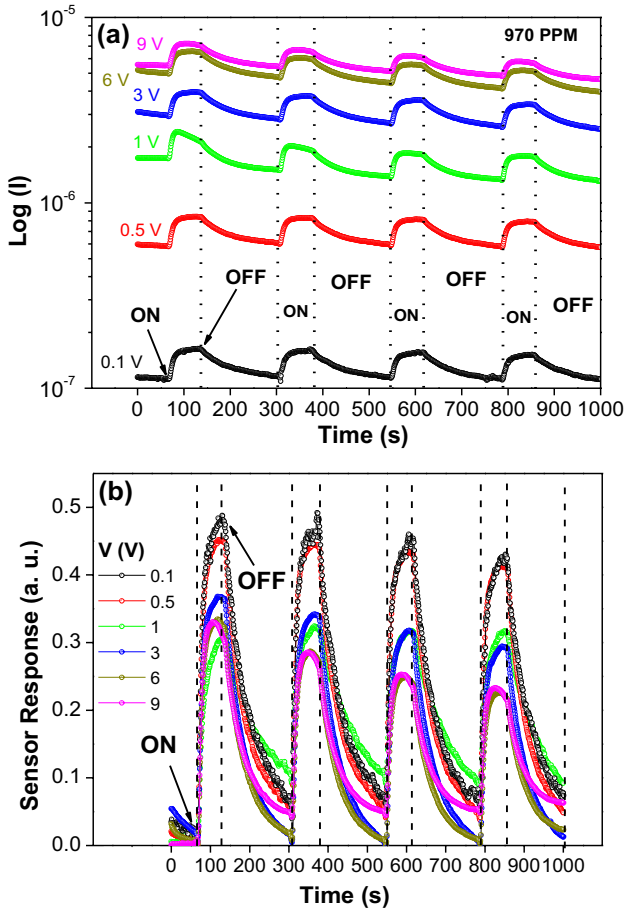

Fig. 5 **a** I-t characteristics of the device when different voltage: 9 V (red), 6 V (dark yellow), 3 V (blue), 1 V (green), 0.5 V (red) and 0.1 V (black). **b** Sensor Response-time under different voltage values: 0.1 V (black), 0.5 V (red), 1 V (green), 3 V (blue), 6 V (dark yellow) and 9 V (pink). All under the same Acetone concentration of 970 PPM

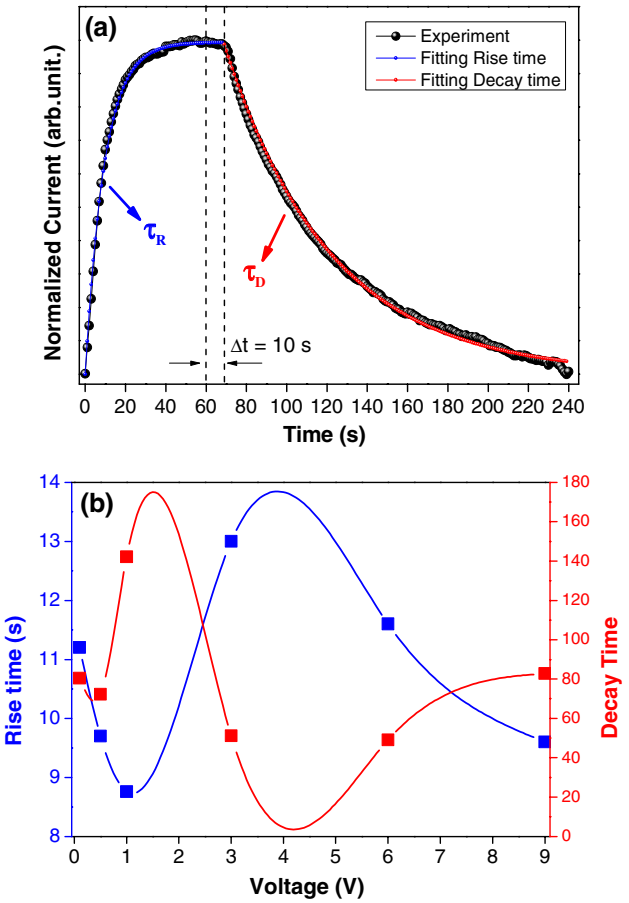

Fig. 6 **a** Fitting for rise and decay time, with time delay variation, represented by Δt, and **b** rise time (blue) and decay time (red), for all tested voltage values. The error resulted from the analysis is smaller than the size of the curve points

$$I(t) = I_0\left(1 - e^{-t/\tau_R}\right), \tag{3}$$

$$I(t) = I_0 e^{-t/\tau_D}, \tag{4}$$

where I_0 is the maximum current value and t is time. Figure 6a displays the current variation of the device subjected to a 240 s cycle. A time variation of about 10 s, was observed between the instant where the Acetone gas flow was interrupted up to the response of this interruption was shown by the sensor, highlighted by the dashed lines. This delay can be related to the time that the Oxygen molecules take to find the vacancy sites to be adsorbed again in the sensitive layer. Therefore, in the decay time, this interval must be taken into account [27].

Rise time (blue) can be seen in Fig. 6b, for all applied voltages. The rise time ranged between 8.7 s and 13 s. By comparison of τ_R values, no significant variation for these applied voltage values were noticed, within the fitting's uncertainty ($r^2 = 0.9992$). Decay time (red) varied from 48.1 s to 142.7 s. Due to different adsorbent sites and defects, one can expect distinctive Oxygen desorption mechanisms, which in turn contributes to a longer time response until the system reaches stability. Moreover, the operation condition of the devices, i.e., at room temperature, also contributes to extend this time response [28]. When under higher applied voltages values, there is a tendency to decrease the decay time, for instance, when increasing the electric field, a higher density of electrons becomes available after gas flow interruption, owing to a thicker depletion layer. In such case, when the gas flow is ceased, there is a favorable condition for rapid oxygen adsorption [29].

As stated previously, Oxygen molecules play a crucial role in determining the physical properties of TCO's NWs, thus, the sensing mechanisms is mostly ruled by Oxygen vacancies on SnO_2's surface [28–30]. Figure 7 depicts a scheme of two different conditions. In Fig. 7a, a condition where the Acetone gas is OFF (Gas OFF condition), i.e.,

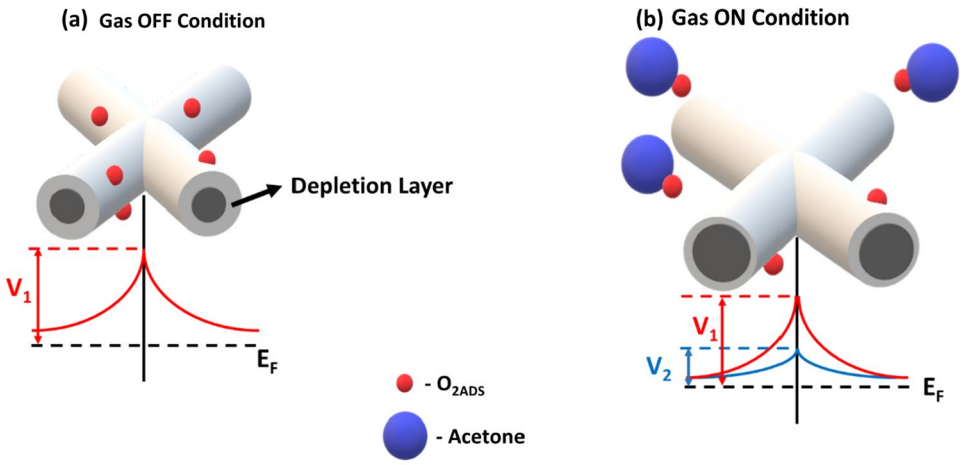

Fig. 7 **a** Gas OFF Condiction: Schematic of a juntion barrier with potential V_1 and Oxygen adsorption (red sphere) for electron transport, **b** Gas ON Condiction: junction barrier is reduced to potencial V_2 and Oxygen desorpiton with Acetona gas exposure (blue sphere)

environment without Acetone, is represented. One can notice the Oxygen molecules (O_{2ADS}, red spheres) adsorbed on the NW surface. The electrons that are available in the Conduction Band (CB) can be captured by the O_{2ADS}. Because of these CB lost electrons, a depletion region and barrier high arise on the surface, preventing electron movement between NW junctions. Since an NW network composes the devices' sensitive layer, the gas sensing properties can be attributed to the presence of countless junctions. Thus, the presence of these homojunctions (SnO_2-SnO_2) lead to a potential barrier (V_1), in such a way that the transport process is affected by it.

When a reducing agent, i.e., a compound that loses or donates electrons (Acetone, blue spheres), is introduced into the system (gas ON condition), it interacts with O_{2ADS} and, by doing it, provokes the discharge of the NW's surface electrons, that once were binded to O_{2ADS}, Fig. 7b. Therefore, electrons are now free to flow back inside of the CB and, due to this charge transference phenomenon, the depletion region gets reduced (when compared to the initial state—gas OFF condition), and charge density increases. In this condition, the potential barrier is represented by V_2 and one can note that it almost disappears in Acetone presence and the device's performance is improved. The contribution of these surface states must be considered in all surfaces, leading to a non-negligible band bending near the nanowire's surface which in turn, results in an effective energy barrier [31].

For all devices studied, a sensor optimized regime was achieved by operation in $V = 0.1$ V ($\tau_R = 11.1$ s and $\tau_D = 79.3$ s). Our device demonstrated an outstanding performance as an Acetone gas sensor, being reinforced by comparison to other sensors that operate at room temperature. For instance, Saraswati and Ruma have achieved a response that ranged between 0.6 and 7% for 500–7000 PPM concentration of Acetone, for a device with a CuO NW network, but much longer rise and decay times of 250 s and 300 s (for 1000 PPM), respectively [4]. Close to the response time values obtained for our sensor, Karthika et al. have reported an Acetone gas sensor using a ZnO thin film with a Rise and decay time of 34 s and 40 s ($\tau_R = 34$ s and $\tau_D = 40$ s) [20]. Jie Zhao et al. built a SnO_2 thin film by a Sol–gel method that presented a sensitivity of about 12 (ratio between gas on and off conditions) under a 1000 PPM Acetone concentration. Rise and decay time were smaller than 20 s and 60 s, respectively [21]. Concerning the same sensitive layer (SnO_2), our sensor achieved a similar response time. Zijing Wang et al. reported an Acetone gas sensor composed by a p–n junction nanocomposites of SnO-SnO_2/ $Ti_3C_2T_x$, operating at room temperature. Sensor response was about 12.1 and rise and decay time was 18 s and 9 s, respectively [22]. In addition to the higher sensor response and shorter decay time presented on their devices, one can see that our sensors had a faster rise time, i.e., a faster response to the presence of Acetone. In summary, the SnO_2 sensors built have a promising application prospect in the detection of acetone gas at room temperature.

4 Conclusion

Summarizing, SnO_2 NW networks were obtained by the VLS growth mechanism. For the device's fabrication process, a MSM architecture was chosen, with tin dioxide and two indium electrical contacts. There was no need of photolithography process, neither clean room environment. The Acetone gas concentration was varied from 50 to 970 PPM and sensor response ranged between 9 and 32% at room temperature. By operating in 0.1 V with a sensitivity of 49% in 970 PPM an optimized regime of the gas sensor was achieved. The rise time varied between 8.7 s and 13 s and decay time ranged between 48.1 s and 142.7 s. The results demonstrated high sensitivity to acetone gas, emphasized by comparison to another studies. In addition, we demonstrated

fast response time, stability and reproducibility, all essential features for a quality sensor.

Acknowledgements The authors thank the financial support from the Brazilian agencies: Grant Nos. 2016/14381-4, 2013/07296-2 and 2019/18963-6, São Paulo Research Foundation (FAPESP) and Grant Nos. 305656/2018-0 and 305615/2014-9 (CNPq).

Funding This work has been funded by Grant Nos. 2016/14381–4, 2013/07296–2 and 2019/18963–6, São Paulo Research Foundation (FAPESP) and Grant Nos. 305656/2018–0 and 305615/2014–9 (CNPq).

Declarations

Conflict of interest The authors declare that they have no conflict of interest.

References

1. Q.A. Drmosh, I.O. Alade, M. Qamar, S. Akbar, Chem. Asian J. **16**, 1519 (2021). https://doi.org/10.1002/asia.202100303
2. V. Saasa, M. Beukes, Y. Lemmer, B. Mwakikunga, Blood ketone bodies and breath acetone analysis and their correlations in Type 2 Diabetes Mellitus. Diagnostics (Basel). **9**(4), 224 (2019). https://doi.org/10.3390/diagnostics9040224
3. B. Yang, N.V. Myung, Tran 2100271, T.-T, 1D metal oxide semiconductor materials for chemiresistive gas sensors: a review. Adv. Electron. Mater. **7**, 2100271 (2021). https://doi.org/10.1002/aelm.202100271
4. K. Saraswati, G. Ruma, A simple approach for sensing and accurate prediction of multiple organic vapors by sensors based on CuO nanowires. Sens. Actuators, B Chem. **335**, 129701 (2021). https://doi.org/10.1016/j.snb.2021.129701 (**ISSN 0925-4005**)
5. Z. Ling, Z. Wen, Room-temperature gas sensing of ZnO-based gas sensor: a review. Sensors Actuators A Phys **267**, 242–261 (2017). https://doi.org/10.1016/j.sna.2017.10.021 (**ISSN 0924–4247**)
6. Y. Zhang, Q. Li, Z. Tian et al., Gas-sensing properties of ITO materials with different morphologies prepared by sputtering. SN Appl. Sci. **2**, 264 (2020). https://doi.org/10.1007/s42452-020-2050-7
7. S.T. Navale, Z.B. Yang, L. Chenshitao, P.J. Cao, V.B. Patil, N.S. Ramgir, R.S. Mane, F.J. Stadler, Enhanced acetone sensing properties of titanium dioxide nanoparticles with a sub-ppm detection limit. Sensors Actuators B Chem **255**, 1701–1710 (2018). https://doi.org/10.1016/j.snb.2017.08.186 (**ISSN 0925–4005**)
8. K. Hongseok, C. Zhicheng, C. Sung-Pil, P. Sunghoon, Improved sub-ppm acetone sensing properties of SnO_2 nanowire-based sensor by attachment of Co3O4 nanoparticles. J. Mater. Rese. Technol. **9**(1), 1129–1136 (2020). https://doi.org/10.1016/j.jmrt.2019.12.094 (**ISSN 2238–7854**)
9. D. Nunes, A. Pimentel, A. Goncalves, S. Pereira, R. Branquinho, P. Barquinha, E. Fortunato, R. Martins, Metal oxide nanostructures for sensor applications. Semicond. Sci. Technol. (2019). https://doi.org/10.1088/1361-6641/ab011e
10. N.A. Adryelle, P.A. Estácio, P. Manuela, A.P. André, J.C. Adenilson, A simple band model for ultraviolet induced ambipolarity in single SnO_2 nanowire devices. PhysE: Low-Dimens Syst Nanostruct **128**, 114607 (2021). https://doi.org/10.1016/j.physe.2020.114607 (**ISSN 1386-9477**)
11. Y. Cheng, P. Xiong, C.S. Yun, G.F. Strouse, J.P. Zheng, R.S. Yang, Z.L. Wang, Mechanism and optimization of pH sensing using SnO_2 nanobelt field effect transistors. Nano Lett **8**(12), 4179–4184 (2008). https://doi.org/10.1021/nl801696b
12. J.R. McGhee, A. Goulas, D.J. Southee, J.S. Sagu, D.S. Engstrøm, J. Wang, D.A. Hutt, P.S.A. Evans, Z. Zhou, K.G.U. Wijayantha, P. Conway, C.J. Carmalt, Indium tin oxide nanowires manufactured via printing and laser irradiation. Appl Mater Today **21**, 100835 (2020). https://doi.org/10.1016/j.apmt.2020.100835 (**ISSN 2352-9407**)
13. R. Gilani, S.U. Rehman, F.K. Butt et al., Elucidating the First-Principles Calculations of SnO_2 Within DFT Framework and Beyond: A Library for Optimization of Various Pseudopotentials. SILICON **10**, 2317–2328 (2018). https://doi.org/10.1007/s12633-018-9766-7
14 D. Soumen, V. Jayaraman, SnO_2: a comprehensive review on structures and gas sensors. Prog Mater Sci **66**, 112–255 (2014). https://doi.org/10.1016/j.pmatsci.2014.06.003 (**ISSN 0079–6425**)
15. P. Nelli, G. Faglia, G. Sberveglieri, E. Cereda, G. Gabetta, A. Dieguez, A. Romano-Rodriguez, J.R. Morante, The aging effect on SnO_2–Au thin film sensors: electrical and structural characterization. Thin Solid Films **371**(1–2), 249–253 (2000). https://doi.org/10.1016/S0040-6090(00)01011-7 (**ISSN 0040–6090**)
16 C. Romain, J. Nicolas, Long term stability of metal oxide-based gas sensors for e-nose environmental applications: an overview. Sensors Actuators B Chem **146**(2), 502–506 (2010). https://doi.org/10.1016/j.snb.2009.12.027 (**ISSN 0925–4005**)
17 G. Korotcenkov, B.K. Cho, Instability of metal oxide-based conductometric gas sensors and approaches to stability improvement (short survey). Sensors Actuators B Chem **156**(2), 527–538 (2011). https://doi.org/10.1016/j.snb.2011.02.024 (**ISSN 0925–4005**)
18. E. Brunet, T. Maier, G.C. Mutinati, S. Steinhauer, A. Köck, C. Gspan, W. Grogger, Comparison of the gas sensing performance of SnO_2 thin film and SnO_2 nanowire sensors. Sensors Actuators B Chem **165**(1), 110–118 (2012). https://doi.org/10.1016/j.snb.2012.02.025 (**ISSN 0925-4005**)
19. A.L.R. Melzi, A.J. Chiquito, The interplay between Arrhenius and hopping conduction mechanisms in a percolating nanowire network. J. Phys. D Appl. Phys. (2016). https://doi.org/10.1088/0022-3727/49/31/315303
20. M. Karthika, V. Manoj, B. Shanmugam, K.K. Rakesh, S. Vijay, K.S. Pramod, Krishnamoorthy Pandiyan, Studies on acetone sensing characteristics of ZnO thin film prepared by sol–gel dip coating. J Alloys Compd **673**, 138–143 (2016). https://doi.org/10.1016/j.jallcom.2016.02.222 (**ISSN 0925–8388**)
21. Z. Jie, H. Li-Hua, G. Shan, Z. Hui, Z. Jing-Gui, Alcohols and acetone sensing properties of SnO_2 thin films deposited by dip-coating. Sensors Actuators B Chem **115**(1), 460–464 (2006). https://doi.org/10.1016/j.snb.2005.10.024 (**ISSN 0925–4005**)
22. W. Zijing, W. Fen, H. Angga, A. Yusuke, H. Takuya, K. Hiromu, K. Hideki, K. Masato, Z. Jianfeng, Y. Shu, SnO-SnO2 modified two-dimensional MXene Ti3C2Tx for acetone gas sensor working at room temperature. J Mater Sci Technol **73**, 128–138 (2021). https://doi.org/10.1016/j.jmst.2020.07.040 (**ISSN 1005–0302**)
23. E.P. de Araújo, A.N. Arantes, I.M. Costa, A.J. Chiquito, Reliable Tin dioxide based nanowire networks as ultraviolet solar radiation sensors. Sensors Actuators A Phys **302**, 111825 (2020). https://doi.org/10.1016/j.sna.2019.111825 (**ISSN 0924-4247**)
24. DeBoer, JR. *Evaluation Methods for Porous Silicon Gas Sensors*. Diss. Georgia Institute of Technology, 2004.
25. G.J. McCarthy, J.M. Welton, X-ray diffraction data for SnO_2 an illustration of the new powder data evaluation methods. Powder Diffr. **4**, 156–159 (1989). https://doi.org/10.1017/S0885715600016638
26. M.O. Orlandi, E.R. Leite, R. Aguiar, J. Bettini, E. Longo, Growth of SnO nanobelts and dendrites by a self-catalytic VLS process. J.

Phys. Chem. B **110**, 6621–6625 (2006). https://doi.org/10.1021/jp057099m
27. W. Maziarz, T. Pisarkiewicz, Gas sensors in a dynamic operation mode. Meas. Sci. Technol. **19**, 055205 (2008). https://doi.org/10.1088/0957-0233/19/5/055205
28. K. Jae-Hun, M. Ali, W.K. Hyoun, W. Ping, S.K. Sang, Design of supersensitive and selective ZnO-nanofiber-based sensors for H2 gas sensing by electron-beam irradiation. Sensors Actuators B Chem **293**, 210–223 (2019). https://doi.org/10.1016/j.snb.2019.04.113 (**ISSN 0925–4005**)
29. H. Ren, H. Huo, P. Wang, C. Wang, S. Liu, M. Shen, H. Sun, M. Ruths, The electric field effect on the sensitivity of tin oxide gas sensors on nanostructured substrates at low temperature. Int. J. Smart Nano Mater. **5**, 257–269 (2014). https://doi.org/10.1080/19475411.2014.995745
30. C. Jiabao, S. Linqi, X. Tengfeng, W. Dejun, L. Yanhong, UV-light illumination room temperature HCHO gas-sensing mechanism of ZnO with different nanostructures. Sensors Actuators B Chem **227**, 220–226 (2016). https://doi.org/10.1016/j.snb.2015.12.010 (**ISSN 0925–4005**)
31. R.A. Simon, H. Kamimura, O.M. Berengue, E.R. Leite, A.J. Chiquito, Disorder induced interface states and their influence on the Al/Ge nanowires Schottky devices. J. Appl. Phys. **114**, 243705 (2013). https://doi.org/10.1063/1.4857035

Publisher's Note Springer Nature remains neutral with regard to jurisdictional claims in published maps and institutional affiliations.